Numerical Astrodynamics

Assignment III

Lorenz Veithen

TU Delft

DELFT UNIVERSITY OF TECHNOLOGY

FACULTY OF AEROSPACE ENGINEERING

AE4868-1

NUMERICAL ASTRODYNAMICS

Numerical Integrators

Lecturer: Dr. D. Dirkx and Dr. Ir. K.J. Cowan

Github repository link:
https://github.com/LorenzVeithen/NumericalAstrodynamics2023_Veithen_Lorenz

April 25, 2023

Q1	Q2	Q3	Q4	Q5	Q6
3h	13h	4h	6h	6h	3h

Lorenz Veithen 5075211

Cooperating Students: Srujan Vaidya (5072034) and Oliver Ross (5008042)

TU Delft Delft University of Technology

Problem 1

1.1 Numerical Solution For Various Timesteps

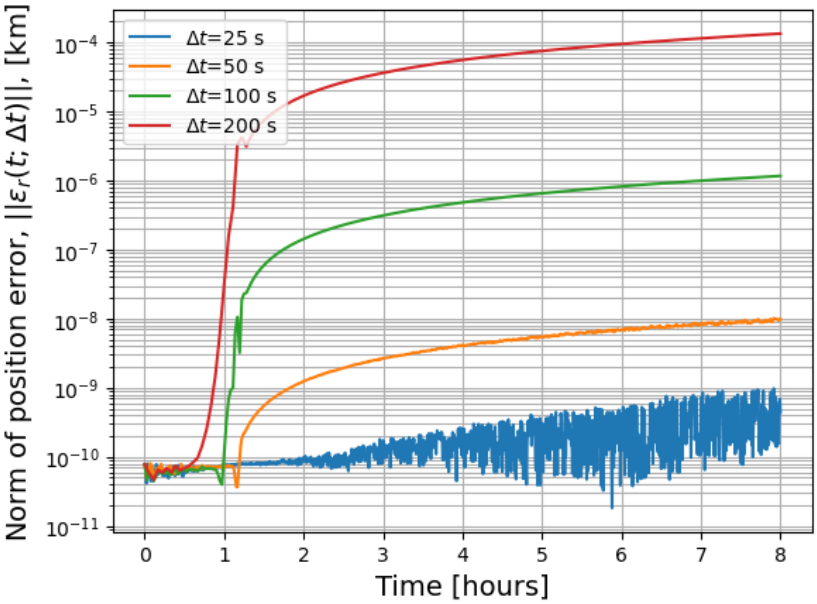

Figure 1.1: Position error in the unperturbed numerical propagation of the Callisto flyby for constant time steps of 25, 50, 100, and 200 seconds. The error is computed from the analytical solution of the trajectory.

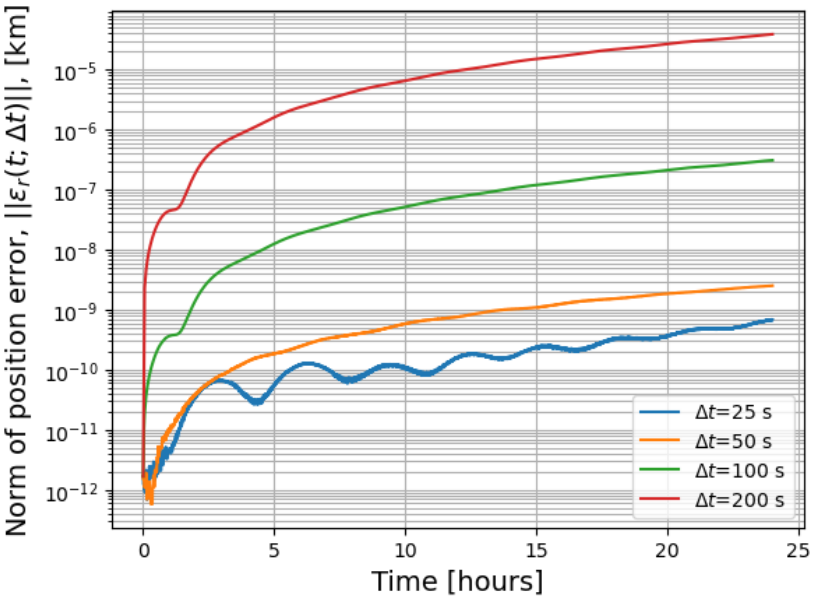

Figure 1.2: Position error in the unperturbed numerical propagation of the orbit around Ganymede for constant time steps of 25, 50, 100, and 200 seconds. The error is computed from the analytical solution of the trajectory.

1.2 Maximum Position Error for Each Time Step

Table 1.1: Maximum position error (in km) of the unperturbed numerical propagation for both the Callisto flyby and Ganymede orbit, as a function of the time step size. The error is computed from the analytical solution of the trajectory.

Case	$\Delta t = 25$s	$\Delta t = 50$s	$\Delta t = 100$s	$\Delta t = 200$s
Callisto Flyby Error [km]	9.766e-10	1.019e-08	1.165e-06	0.0001337
Ganymede Orbit Error [km]	6.87e-10	2.526e-09	3.103e-07	3.905e-05

1.3 Dominance of Truncation Error Based on Maximum Position Error

RKF7(8) is of order 7 (GTE), meaning that in the truncation error region $||\boldsymbol{\epsilon_r}|| \sim \mathcal{O}(\Delta t^7)$ and dividing Δt by 2 should divide $||\boldsymbol{\epsilon_r}||$ by 128. From Tab. 1.2, it is clear that the error for $\Delta t = 25$s is dominated by rounding errors (in both cases) rather than truncation errors, because 10 and 3.7 $<<$ 128 (whereas 114-126 are much closer). For the Callisto flyby, a ratio of 114.4 is within 11% of 128; this variation could be explained by the neglected higher order terms in Eq. (1.2) ($\boldsymbol{K}_8(t_{max})$ same for all Δt: max error at end epoch for all curves).

$$r(\Delta t_1, \Delta t_2) = \frac{\max\limits_t ||\epsilon_r(t; \Delta t_1)||}{\max\limits_t ||\epsilon_r(t; \Delta t_2)||} \tag{1.1}$$

Table 1.2: Ratios of maximum error of the unperturbed numerical propagation obtained with different timesteps.

Case	$r(50, 25)$	$r(100, 50)$	$r(200, 100)$
Callisto Flyby	10.43	114.4	114.8
Ganymede Orbit	3.677	122.8	125.9

1.4 Dominance of Truncation Error Based on Change in Position Error as a Function of Time

The LTE[1] follows Eq. (1.2), which is smooth ($\boldsymbol{K}_p$ smooth), and builds up to a 7th order GTE[2]. As the multiplication and addition smooth of functions is smooth, a smooth behaviour of $||\boldsymbol{\epsilon_r}(t; \Delta t)||$ is expected if the LTE is dominant. All Δt curves in Fig. 1.1 (Callisto) exhibit rounding errors at the start (inherently random variations), but only $\Delta t = 25$s is strongly dominated by rounding errors throughout the entire phase, while $\Delta t = 50$s is slightly subject to them (roughness). In Fig. 1.2 (GCO500), only $\Delta t = 25, 50$s show strong rounding errors at the start of the propagation, and are subject to them weakly throughout the trajectory (roughness).

$$||\boldsymbol{\epsilon_r}(t + \Delta t; \Delta t)|| = \sum_{i=8}^{\infty} \frac{(\Delta t)^i}{i!} \frac{d^i}{dt^i}(\boldsymbol{y}(t)) \approx \boldsymbol{K}_8(t)(\Delta t)^8 \qquad \boldsymbol{K}_8(t) = \frac{1}{8!}\frac{d^8}{dt^8}(\boldsymbol{y}(t)) \tag{1.2}$$

1.5 Maximum Error As a Function of the Time Step Size

Based on Fig. 1.3, it can be concluded that the optimal time step is about 36-40s for the Callisto flyby, and about 45-50s for the Ganymede orbit. In a log-log plot, polynomials of the form of Eq. (1.2) (and the build up

[1] Local Truncation Error
[2] Global Truncation Error

to 7th order GTE) are straight lines. For lower Δt than mentioned above, the curve is not linear anymore and starts to show the randomness and levelling off expected from rounding errors due to machine precision.

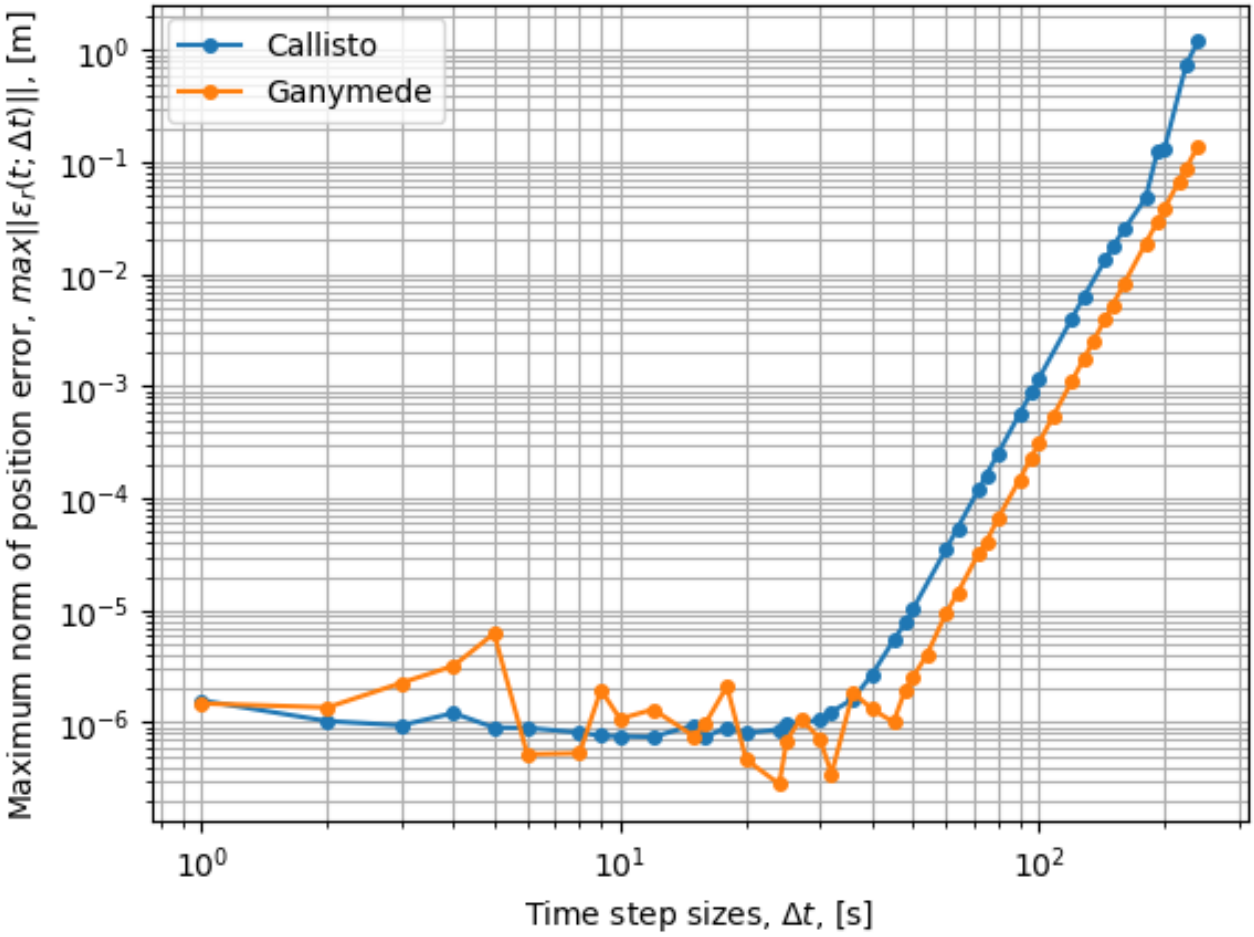

Figure 1.3: Maximum position error as a function of the time step size, Δt.

Problem 2

2.1 Behaviour of Error with Variable Time Step Solver

The variable time step solutions generally behave as expected: (1) a smaller tolerance (both relative and absolute) results in a smaller error, and (2) the overall trend shows that $||\epsilon_r(t)||$ grows with time. Considering (2), the tolerance only ensures that the LTE is smaller than a value ϵ^*_{req} from Eq. (2.1), but $||\boldsymbol{\epsilon_r}(t)||$ will grow due to the build up of local errors. Rounding errors are visible for the 1e-12 tolerance curve during the entirety of the GCO500 case (seen from the roughness). ToL=1e-12 for the Callisto flyby shows rounding error dominance in the first 2h, but LTE's become dominant shortly after passing the pericenter because the position ($\sim y$ in Eq. (2.1)) becomes large, increasing $\epsilon_{rel}y$ and ϵ^*_{req}, and rounding becomes less important.

$$\epsilon^*_{req} = \epsilon_{rel}y + \epsilon_{abs} = \epsilon(y+1) \qquad \epsilon_{rel} = \epsilon_{abs} \tag{2.1}$$

$$\epsilon_{GTE}(t) = \sum_{i=0}^{i=n_t} \epsilon_{LTE}(t_i + \Delta t) \qquad n_t\text{, number of time steps until time t} \tag{2.2}$$

Reducing the tolerance is expected to result in a reduction of the $||\boldsymbol{\epsilon_r}(t)||$ by about the same order of magnitude, because the latter results from the build up of LTE over time (Eq. (2.2)). Dividing ϵ by 100 will divide ϵ^*_{req} by the same factor, assuming that y does not change much. This smaller ϵ^*_{req} will result in more time steps, N (Tab. 2.1). Assuming that N doubles with a tolerance 100 times smaller, this would result in an error about 50 times smaller (Eq. (2.2), equidistant curves). However, the curves are not in equidistant in Fig. 2.1, contrary to Fig. 2.2. This behaviour could arise from the TLE dominance assumption of the $\Delta t-$control algorithm being invalid at the pericenter passage: the state ($\sim y$) becomes small, ϵ^*_{req} and Δt decrease drastically, and the 8th order integrator (RKF7(**8**)) might reach rounding errors for tolerances of 1e-10 and 1e-12, yielding inappropriate Δt choice, and resulting in a different distance between the curves, sustained over the rest of the integration.

Table 2.1: Number of time steps per propagation for tolerance of 1e-6, 1e-8, 1e-10, and 1e-12, for the Callisto flyby and the GCO500 cases. It is clear that the number of time steps roughly doubles when the tolerance is divided by a factor 100.

Case	ToL = 1e-6	ToL = 1e-8	ToL = 1e-10	ToL = 1e-12
Callisto flyby	21	32	52	98
GCO500	255	516	1078	2280

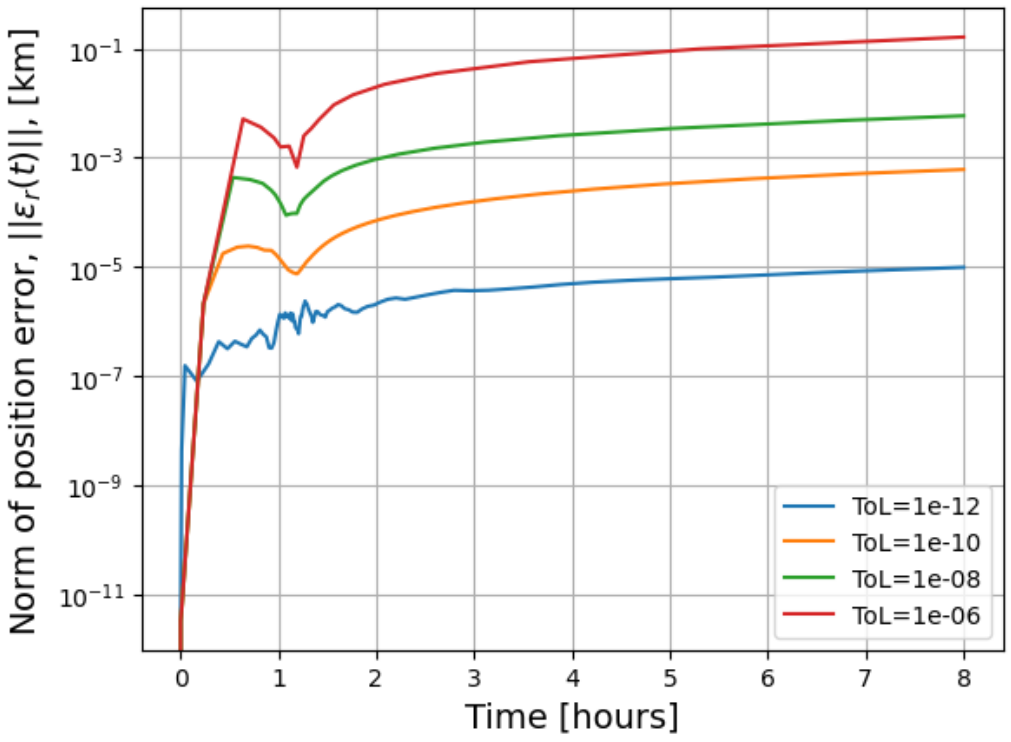

Figure 2.1: Perturbed Callisto flyby position error of the RKF5(6) variable time step integration using tolerances of 1e-12, 1e-10, 1e-8, and 1e-6, with respect to the benchmark RKF7(8) fixed time step with $\Delta t = 1$s. The absolute and relative tolerances are taken equal.

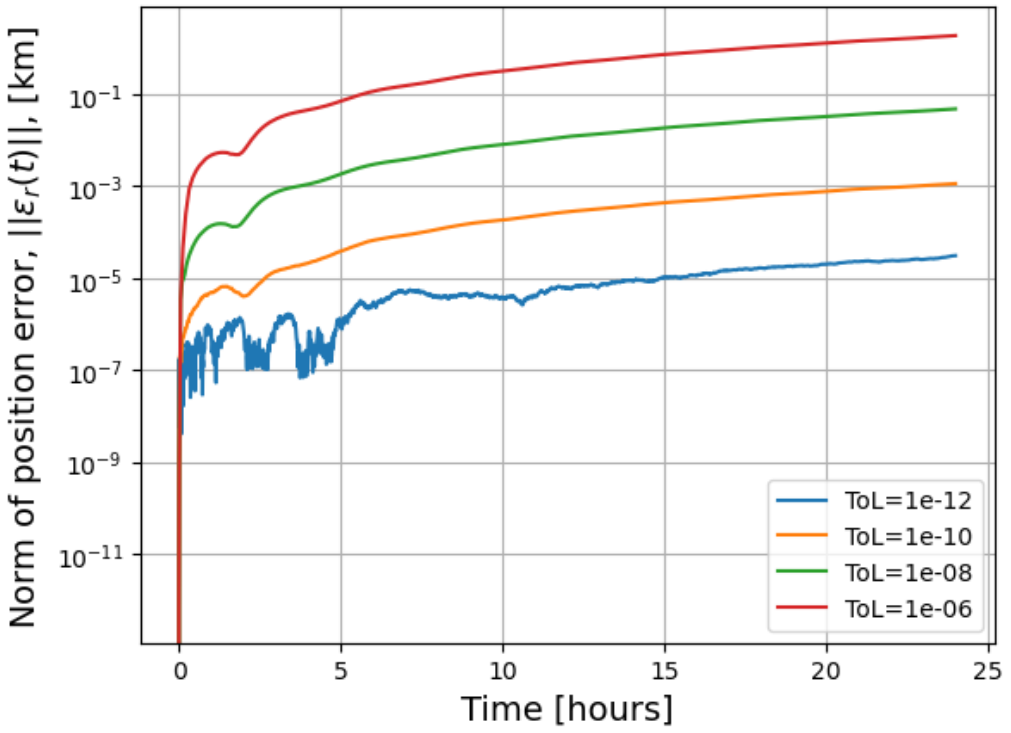

Figure 2.2: Perturbed Ganymede orbit position error of the RKF5(6) variable time step integration using tolerances of 1e-12, 1e-10, 1e-8, and 1e-6, with respect to the benchmark RKF7(8) fixed time step with $\Delta t = 5$s. The absolute and relative tolerances are taken equal.

2.2 Time Step Variation as a Function of Time

Considering the Callisto flyby in Fig. 2.4, Δt becomes smaller when JUICE reaches higher velocities as it goes through the pericenter (Fig. 2.5). Following, Δt increases again after $\approx$ 1.1h, as JUICE's velocity decreases and the dynamics become less constraining. For the GCO500 case, the overall trend shows a pretty constant Δt throughout the orbit. This is expected as the orbit is near-circular, meaning that the dynamics are similar throughout the entire orbit (Fig. 2.7). In both cases, sharp decreasing spikes of Δt are observed (3 close at the perigee for the flyby), without direct link to the dynamical or acceleration environment. These spikes reflect the components of the state vector going through 0, which reduces ϵ^*_{req} of the component and results in a smaller step Δt. For the GCO500 case, this is shown by Figs. 2.8 and 2.9.

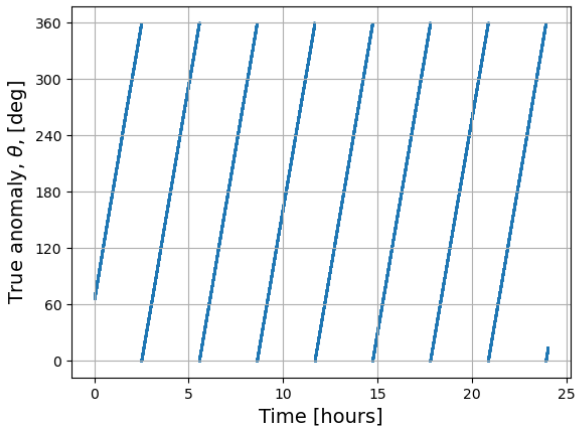

Figure 2.3: True anomaly as a function of time of the benchmark solution for the Ganymede orbit case. This plot was used to determine the orbit of JUICE to be approximately 3.055h.

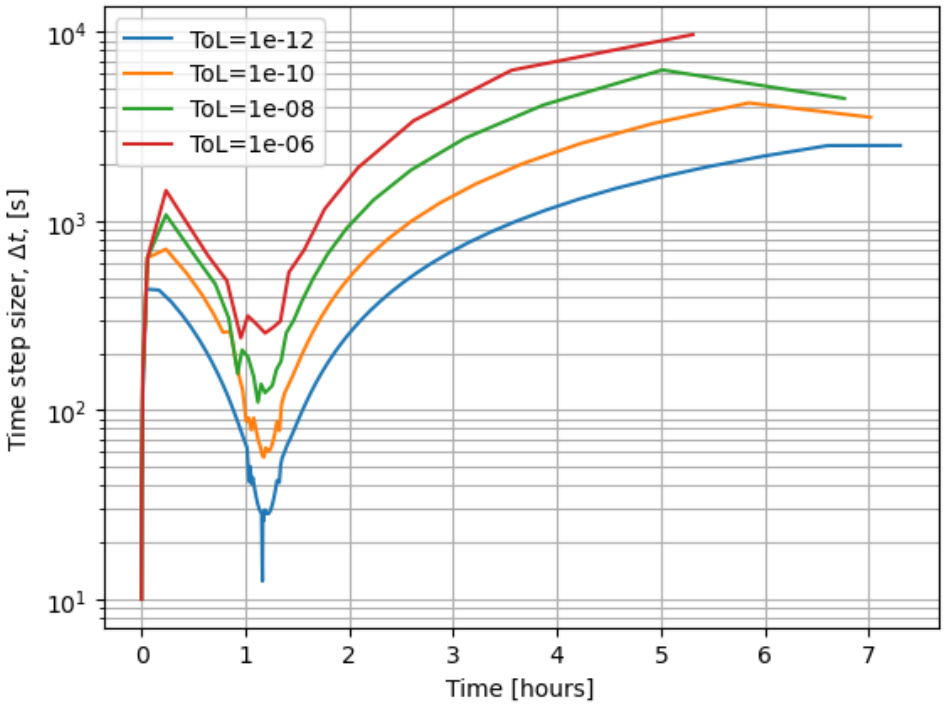

Figure 2.4: Time step size, Δt, as a function of time for the perturbed Callisto flyby using a RKF5(6) variable time step integration with tolerances of 1e-12, 1e-10, 1e-8, and 1e-6. The absolute and relative tolerances are taken equal. The time step to be taken at a particular time is plotted, meaning that the curves stop before reaching the final time of 8h.

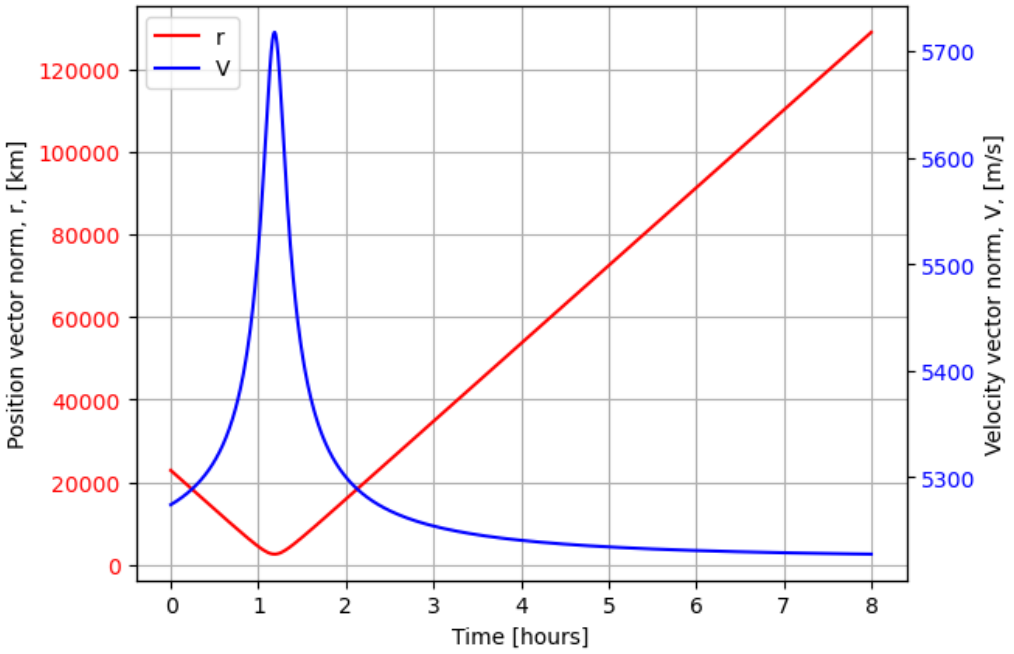

Figure 2.5: Position and velocity vector magnitudes as functions of time during the Callisto flyby. The time step size then becomes significantly when the velocity becomes larger and JUICE goes through the pericenter.

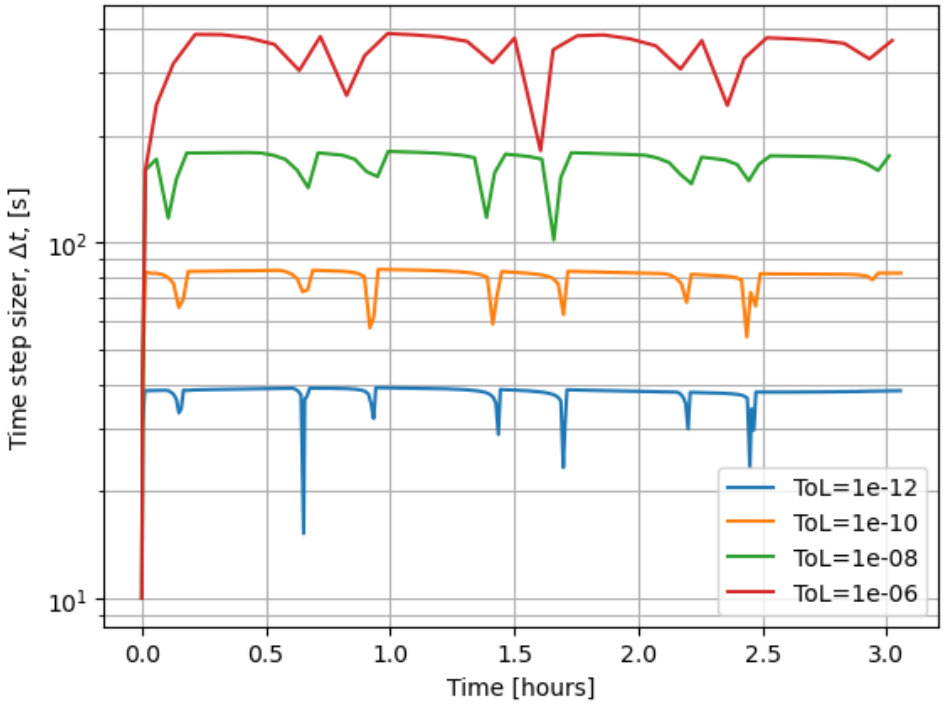

Figure 2.6: Time step size, Δt, as a function of time for the perturbed Ganymede orbit using a RKF5(6) variable time step integration with tolerances of 1e-12, 1e-10, 1e-8, and 1e-6. The absolute and relative tolerances are taken equal.

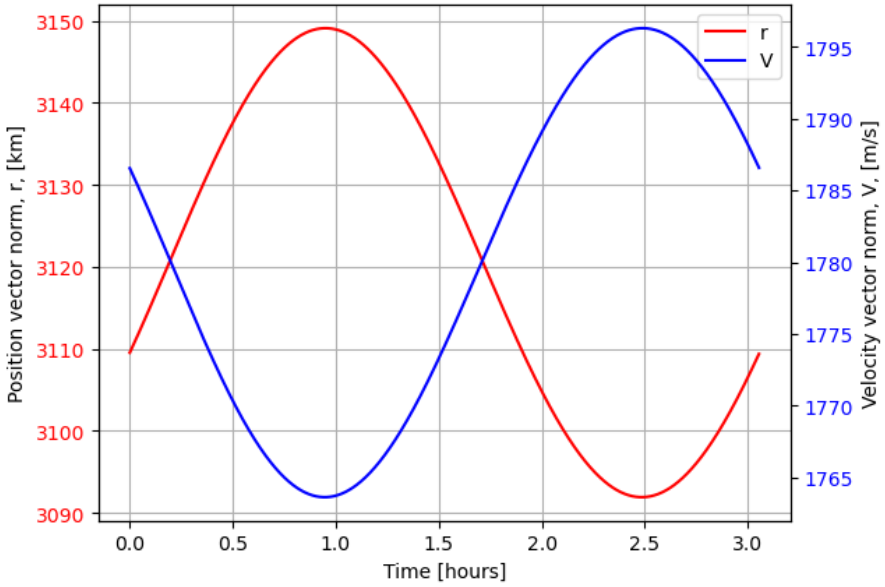

Figure 2.7: Position and velocity vector magnitudes as functions of time during the GCO500. No large changes in position and velocity magnitudes, comparable to the Callisto case, are observed.

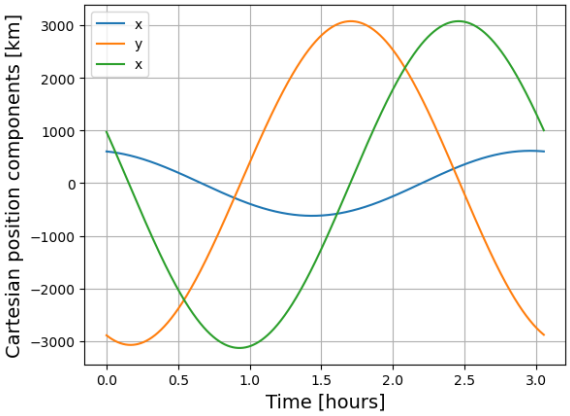

Figure 2.8: Cartesian components of JUICE position in the GCO500 orbit, as a function of time.

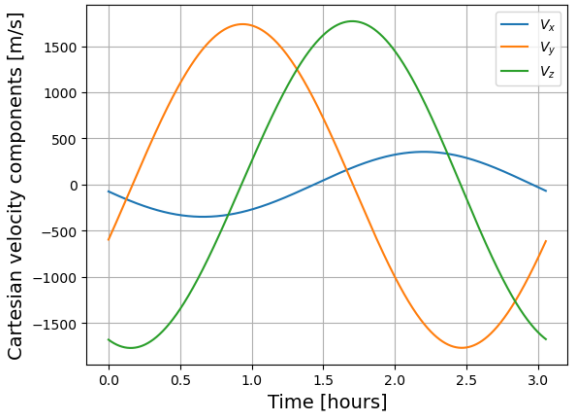

Figure 2.9: Cartesian components of JUICE velocity in the GCO500 orbit, as a function of time.

Table 2.2: Time of the sharp decrease in time step size and associated component of the state vector going through zero, for the GCO500 case.

Time of Δt Spikes [hours]	**State Component Zero**
0.15	z & V_y
0.66	x
0.94	y
1.44	V_x
1.70	z
2.20	x
2.46	y & V_z
2.96	V_x

Table 2.3: Time of the sharp decrease in time step size and associated component of the state vector going through zero, for the Callisto flyby case. Note that the velocity components never go through zero.

Time of Δt Spikes [hours]	**State Component Zero**
1.05	y
1.17	x
1.32	z

2.3 Prove the Explanations

To show the effect of the state's zeros, ϵ_{rel} is put to zero, and only ϵ_{abs} is active (the rest is kept the same), Fig. 2.10. The unperturbed Callisto case was run to show that the trend arises from the overall dynamics, Fig. 2.12.

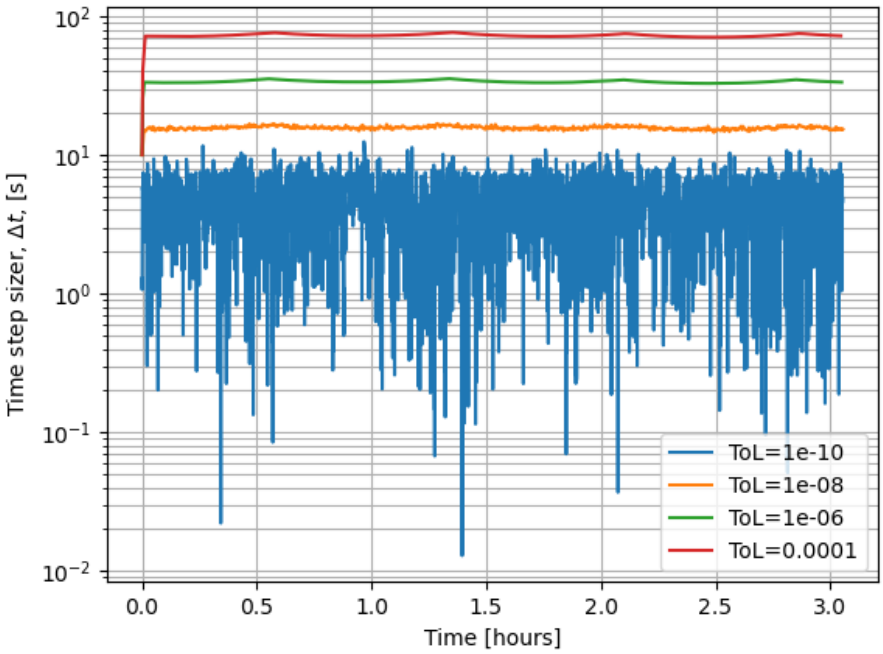

Figure 2.10: Time step size, Δt, as a function of time for the perturbed GCO500 case using a RKF5(6) variable time step integration with absolute tolerance of 1e-10, 1e-8, 1e-6, and 1e-4. *The relative tolerances are taken as zero, as this removes the impact of the state vector on* ϵ^*_{req}*, seeing Eq.* (2.1). **Result:** it is clear that the spikes disappeared (1e-10 is subject to rounding errors), showing that they were indeed occurring due to the components of the state values going to zero (based on the correlation shown earlier, and the fact that they disappear here). A similar result can be obtained for the Callisto case. (**proves** explanation).

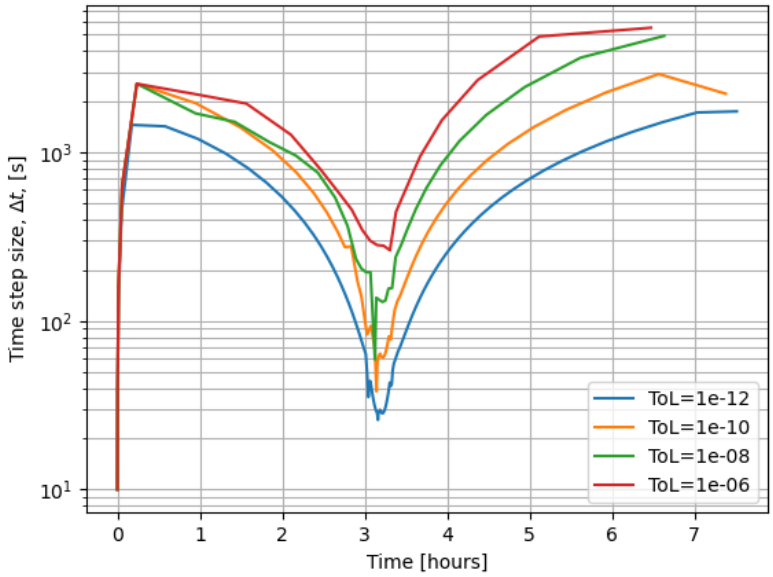

Figure 2.11: Time step size, Δt, as a function of time for the Callisto flyby case using a RKF5(6) variable time step integration with tolerances of 1e-10, 1e-8, 1e-6, and 1e-4. The relative and absolute tolerances are taken equal. *The initial state was shifted by 2 hours*. **Result:** this shows that the lower Δt are also shifted by 2 hours, meaning that they are still aligned with the perigee, as shown before.

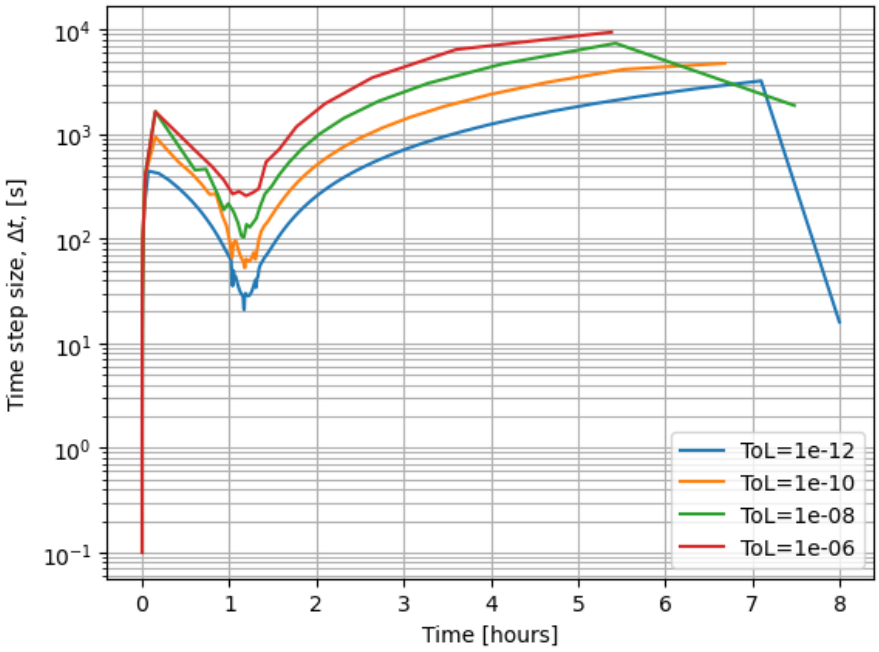

Figure 2.12: Time step size, Δt, as a function of time for the Callisto flyby case using a RKF5(6) variable time step integration with tolerances of 1e-10, 1e-8, 1e-6, and 1e-4. The relative and absolute tolerances are taken equal. *The perturbations were turned off to show that the lower time steps do not arise from the influence of any perturbations, but only from the pass through the pericenter.* **Result:** removing the perturbations reduces the magnitude of the spikes (which arise from the zeroes in the state as shown earlier), but do not remove the overall trend, meaning that it arises from the overall dynamics, and hence the pericenter passage (**proves** explanation).

Problem 3

3.1 Error of Variable Time Step Solver

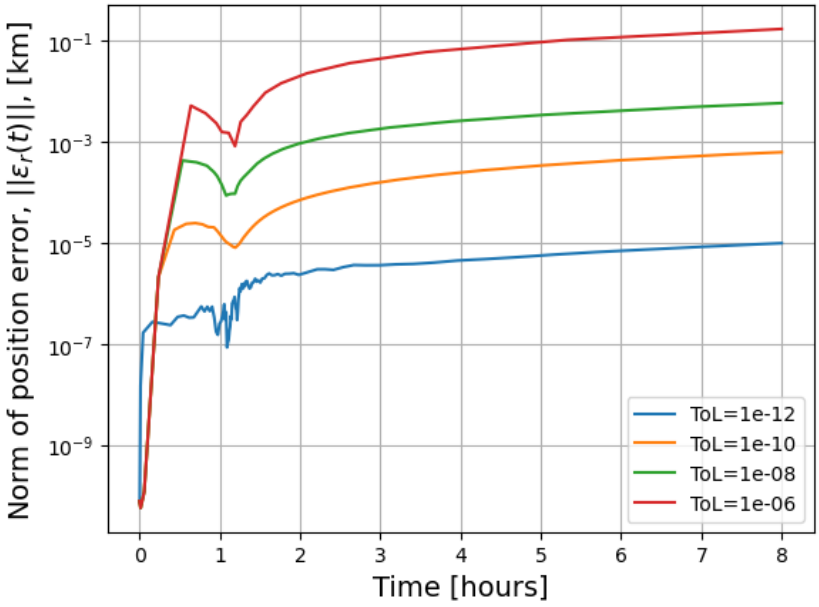

Figure 3.1: Unperturbed Callisto flyby position error of the RKF5(6) variable time step integration using tolerances of 1e-12, 1e-10, 1e-8, and 1e-6, with respect to the analytical solution. The absolute and relative tolerances are taken equal.

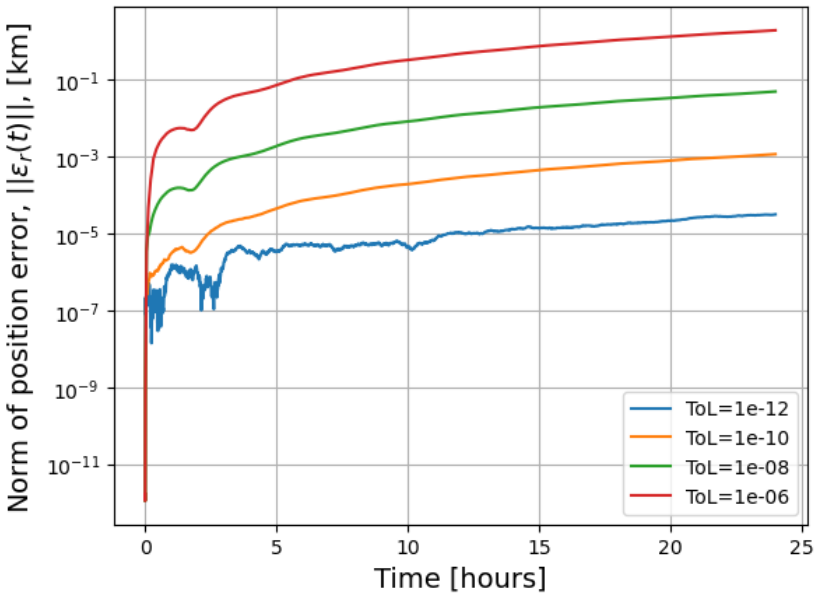

Figure 3.2: Unperturbed Ganymede orbit position error of the RKF5(6) variable time step integration using tolerances of 1e-12, 1e-10, 1e-8, and 1e-6, with respect to the analytical solution. The absolute and relative tolerances are taken equal.

3.2 Discussion

The unperturbed case error behaviour is similar to the results from Q2: (1) the error grows as a function of time in both cases; (2) a similar dimple can be seen around 1h for the Callisto flyby and 2h for the GCO500; (3) rounding errors dominate the $ToL = 1e - 12$ curves at the start of the Callisto flyby and during the entire GCO500, for both; (4) the change in error when dividing the tolerance by a factor 100 is also very similar (also the unequal spacing between the curves of the Callisto flyby). Furthermore, about the same order of magnitude is found both on Figs. 2.1 and 3.1, and on Figs. 2.2 and 3.2, respectively. This is also seen in Tabs. 3.1 and 3.2. Hence, for both the flyby and the GCO500 cases, the unperturbed problem can be used to compare different integrators, given that the trajectories are indeed similar, to ensure fair comparison (see Fig. 3.3 for Callisto).

Table 3.1: Maximum position error for the perturbed (Q2, compared to a benchmark) and the unperturbed (Q3, compared to the analytical solution) Callisto flyby numerical solutions. The small difference in the maximum position errors between the perturbed and unperturbed cases, arises from the slightly different trajectories of both models.

Tolerance	**Unperturbed [km]**	**Perturbed [km]**
1e-6	1.690E-1	1.640E-1
1e-8	5.780E-3	5.880E-3
1e-10	6.178E-4	6.087E-4
1e-12	9.820E-6	9.764E-6

Table 3.2: Maximum position error for the perturbed (Q2, compared to a benchmark) and the unperturbed (Q3, compared to the analytical solution) GCO500 numerical solutions. The small difference in the maximum position errors between the perturbed and unperturbed cases, arises from the slightly different trajectories of both models.

Tolerance	**Unperturbed [km]**	**Perturbed [km]**
1e-6	1.871e+0	1.892e+0
1e-8	4.810e-2	4.805e-2
1e-10	1.136e-3	1.135e-3
1e-12	3.098e-5	3.082e-5

The lack of difference between the perturbed and the unperturbed error behaviours can be explained for both cases separately. For the GCO500 case, the 2nd largest acceleration is 3 orders of magnitude smaller (see Fig. 3.5), which could be significant for long term missions but is barely visible on 24h (8 orbits). For the Callisto flyby, the Jupiter SH acceleration becomes dominant after 4.5h (see Fig. 3.4), but the fast dynamics give a lot of inertia to the spacecraft, meaning that the perturbing accelerations have a lesser effect than for the GCO500 case within the time considered (1e-3 m/s/s acceleration during 4h gives at most 14.4 m/s of delta-V). For both, the unperturbed dynamics are therefore close to the perturbed one, and the integrator hence treats both similarly.

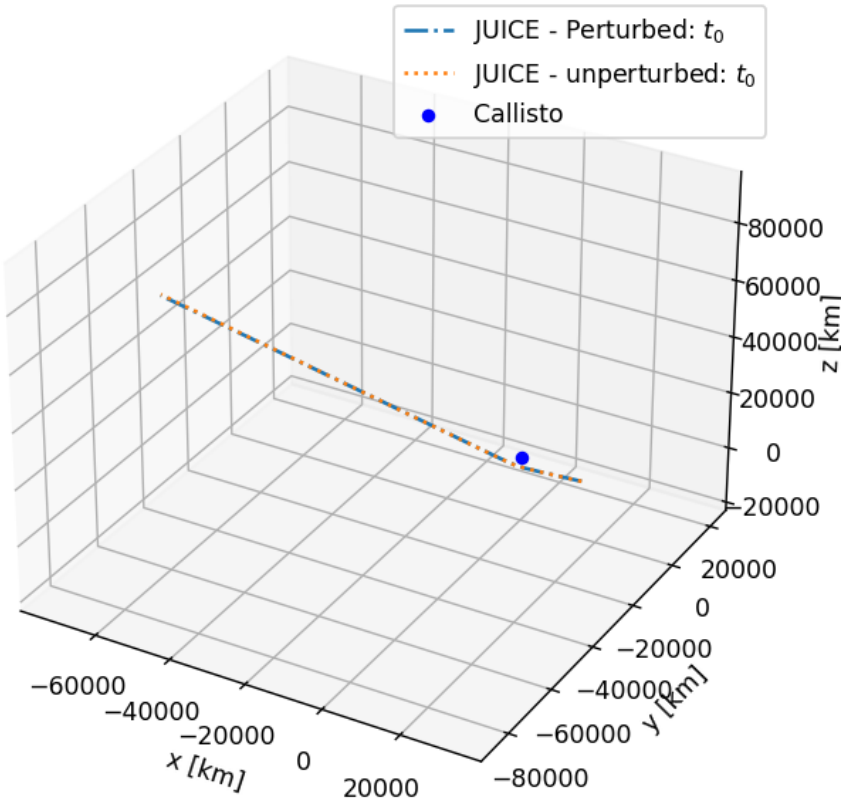

Figure 3.3: 3D plot of the perturbed and unperturbed trajectory for the Callisto flyby. It is clear that the overall trajectory is about the same for both the perturbed and unperturbed cases, meaning that the discussion presented above is based on a fair comparison. A similar figure can be obtained for the GCO500 case.

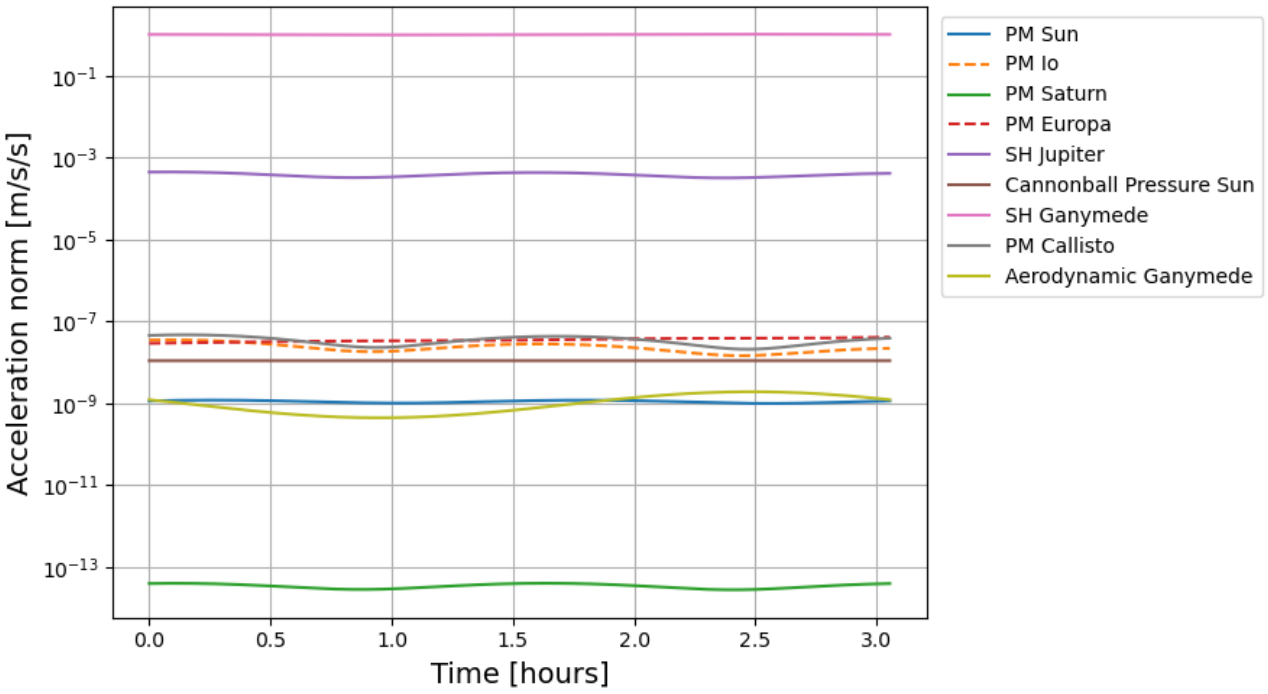

Figure 3.4: Norm of accelerations present in the acceleration model for the GCO500 based on the benchmark solution with a fixed time step of $\Delta t = 5$s.

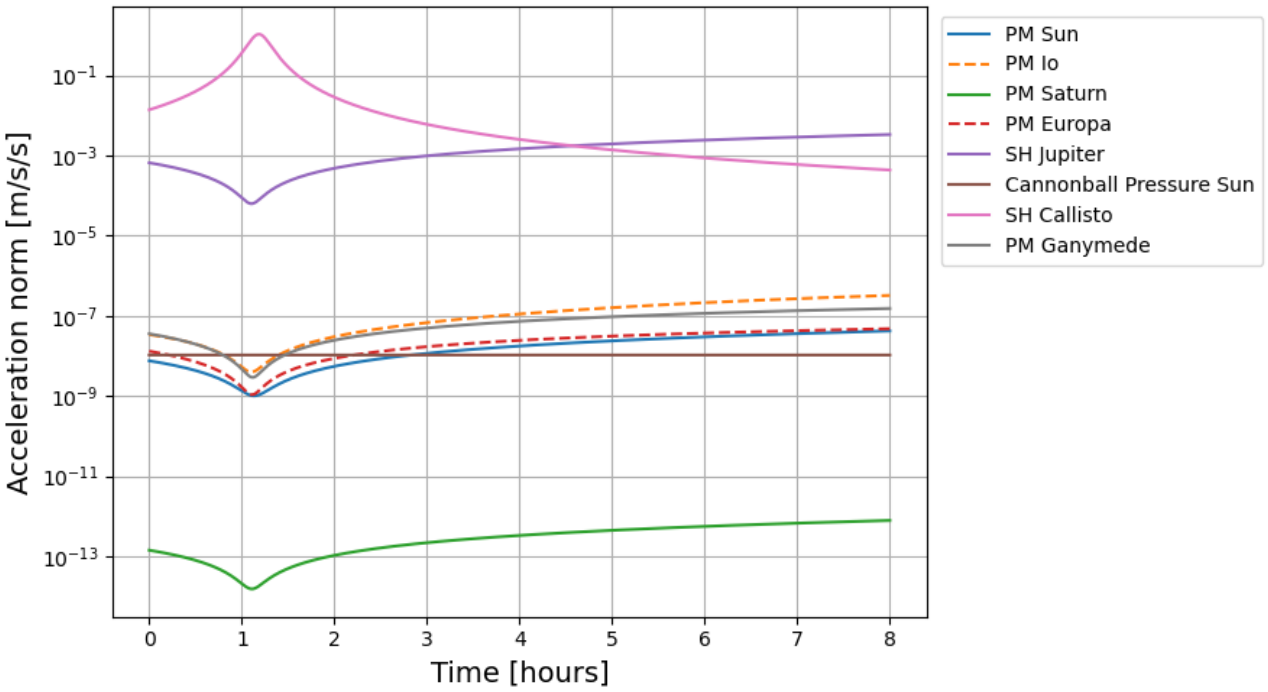

Figure 3.5: Norm of accelerations present in the acceleration model for the Callisto flyby based on the benchmark solution with a fixed time step of $\Delta t = 1$s.

Problem 4

4.1 Closest Approach Time

$$t_c - t_0 = 4265\ s \tag{4.1}$$

4.2 Different Sets of Integration

From Tabs. 4.1 and 4.2, and the Figs presented below, the maximum position error is at least one order of magnitude larger for the t_0-24h propagation (perturbed and unperturbed), compared to the t_0 propagation. Furthermore, the error is smaller for the propagation starting from t_c. The specified tolerance in variable time-step methods permits to control the LTE to be below some threshold at each time step (through Eq. (2.1)), but the longer the propagation time, the more the LTE builds up towards a larger GTE. This results in larger maximum position errors for longer propagation times. Additionally, the pericenter passage is the most constraining part of the trajectory to be resolved, due to its fast dynamics (also see Fig. 1.1, the error blows up around the closest passage only). This means that a slight difference in state at the time of closest passage t_c, due to small deviations building up prior to the approach, will result in large errors over time. It is therefore naturally expected that the error for $t > t_c$ is largest for t_0-24h, and that it is the smallest for t_c (independent of perturbed/unperturbed case). Considering the effect of the perturbations, in Tabs. 4.3 and 4.5, the t_0-24h propagation clearly stands out, indicating that the trajectory may be different than expected, which is confirmed by Fig. 4.7: the unperturbed trajectory is completely different and therefore experiences different dynamics (perturbations are necessary for the flyby since $t0$-24h). This results in a different error behaviour. Additionally, Tab. 4.3 also shows that the t_c propagation is more affected by perturbations than the t_0 one.

Table 4.1: Order of magnitude of the maximum position error (in km) for the unperturbed Callisto flyby with tolerances of 1e-6, 1e-8, 1e-10, and 1e-12, with initial propagation times of t_0, t_c and $t_0 - 24$h.

Initial times	ToL=1e-6	ToL=1e-8	ToL=1e-10	ToL=1e-12
t_0	1.690E-1	5.780E-3	6.178E-4	9.820E-6
t_c	7.594E-2	4.699E-3	2.477E-4	6.203E-6
$t_0 - 24$h	8.389E+0	1.884E-1	3.132E-3	1.140E-4

Table 4.2: Order of magnitude of the maximum position error (in km) for the perturbed Callisto flyby with tolerances of 1e-6, 1e-8, 1e-10, and 1e-12, for initial propagation times of t_0, t_c and $t_0 - 24$h.

Initial times	ToL=1e-6	ToL=1e-8	ToL=1e-10	ToL=1e-12
t_0	1.640E-1	5.880E-3	6.087E-4	9.764E-6
t_c	7.463E-2	4.359E-3	2.098E-4	5.371E-6
$t_0 - 24$h	1.776E+0	2.702E-1	2.227E-3	7.258E-5

Table 4.3: Percentage difference between the maximum position error of the perturbed and unperturbed Callisto flyby with tolerances of 1e-6, 1e-8, 1e-10, and 1e-12, and for initial propagation times of t_0, t_c and $t_0 - 24$h. Computed based on $(e_{perturbed} - e_{unperturbed})/e_{perturbed}$.

Initial times	ToL=1e-6	ToL=1e-8	ToL=1e-10	ToL=1e-12
t_0	3.05%	-1.70%	1.49%	0.57%
t_c	1.76%	7.80%	18.06%	15.49%
$t_0 - 24$h	372.35%	-30.27%	40.64%	57.07%

Table 4.4: Times of closest passage to Callisto in the unperturbed propagation. The time is indicated with respect to the initial start phase t_0, computed from $t_p - t_0$ (in seconds). The reference value given by SPICE is 4265s.

Initial times	ToL=1e-6	ToL=1e-8	ToL=1e-10	ToL=1e-12
t_0	4283.309	4283.027	4245.384	4258.596
t_c	4265.000	4265.000	4265.000	4265.000
$t_0 - 24$h	4406.740	4259.892	4248.551	4258.758

Table 4.5: Times of closest passage to Callisto in the perturbed propagation. The time is indicated with respect to the initial start phase t_0, computed from $t_p - t_0$ (in seconds). The reference value given by SPICE is 4265s.

Initial times	ToL=1e-6	ToL=1e-8	ToL=1e-10	ToL=1e-12
t_0	4283.402	4283.225	4245.951	4261.890
t_c	4265.000	4265.000	4265.000	4265.000
$t_0 - 24$h	-4197.777	-753.288	-577.330	16.419

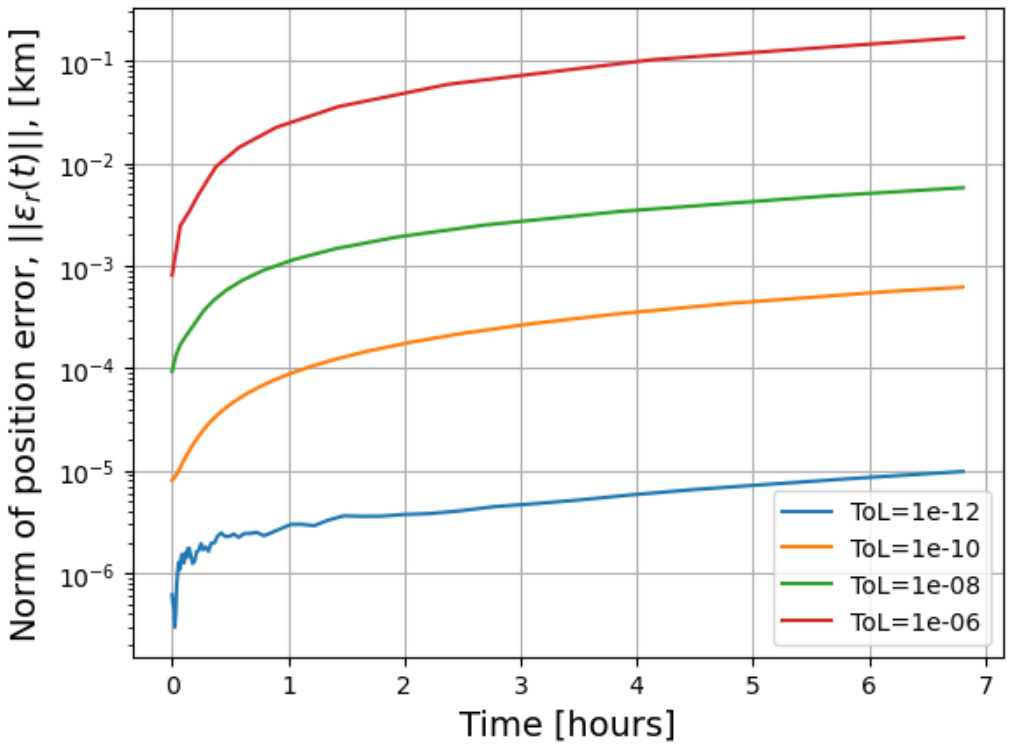

Figure 4.1: Unperturbed Callisto flyby position error of the RKF5(6) variable time step integration using tolerances of 1e-12, 1e-10, 1e-8, and 1e-6, with respect to the analytical solution. The initial propagation time is set to t_0 (like in Q2), but the error is plotted from t_c only.

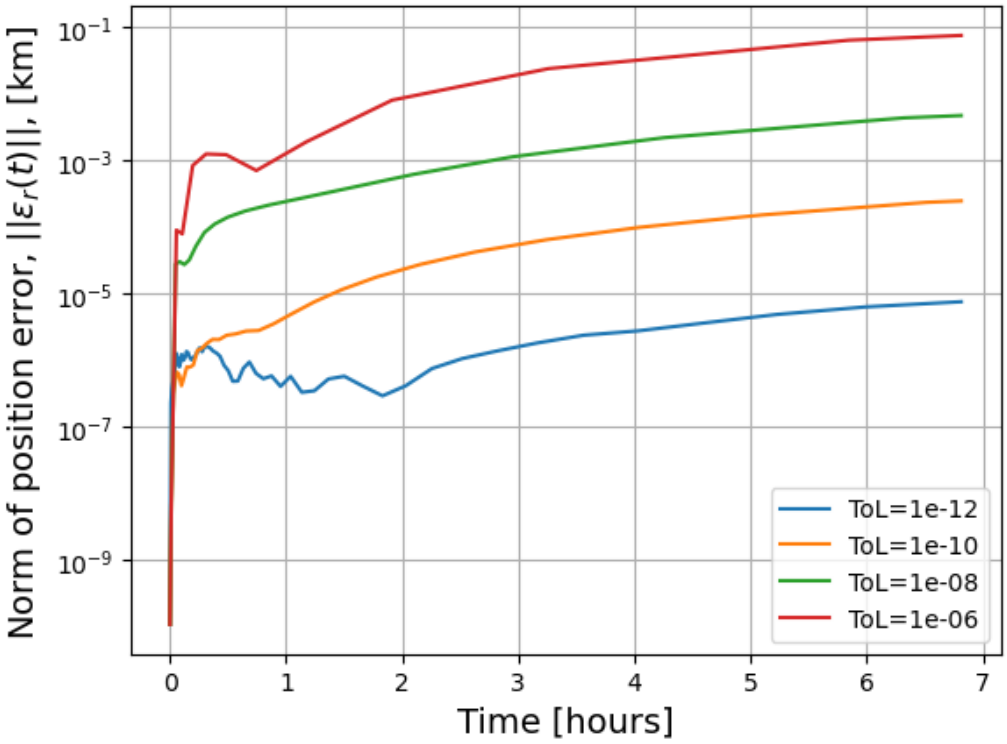

Figure 4.2: Unperturbed Callisto flyby position error of the RKF5(6) variable time step integration using tolerances of 1e-12, 1e-10, 1e-8, and 1e-6, with respect to the analytical solution. The initial propagation time is set to t_c, but the error is plotted from t_c only.

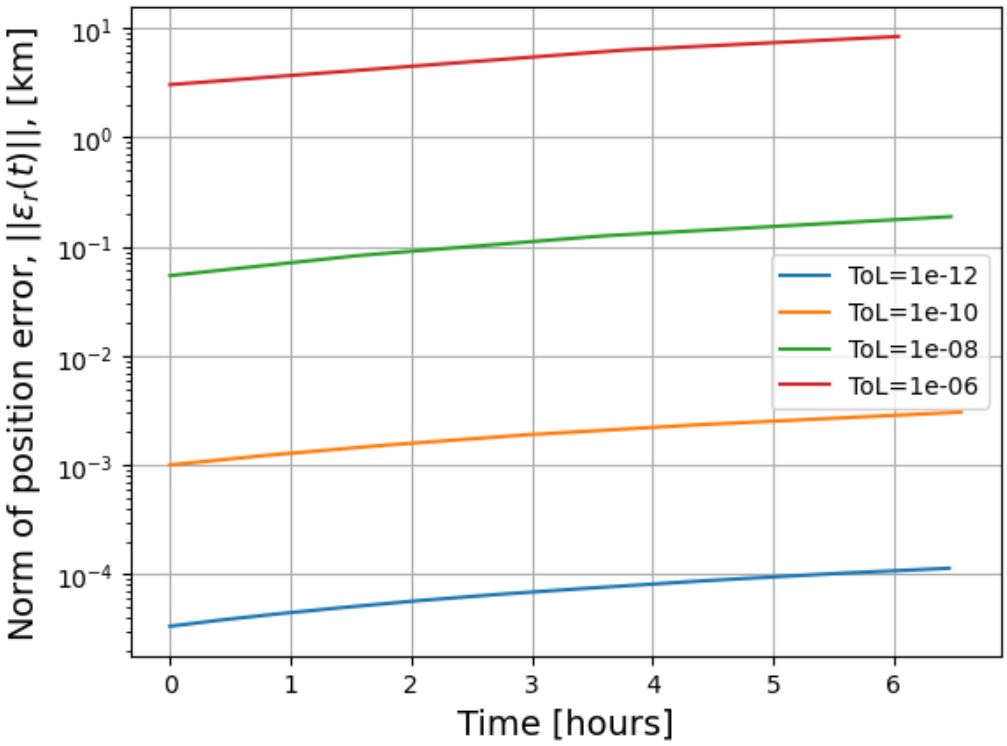

Figure 4.3: Unperturbed Callisto flyby position error of the RKF5(6) variable time step integration using tolerances of 1e-12, 1e-10, 1e-8, and 1e-6, with respect to the analytical solution. The initial propagation time is set to $t_0 - 24$h, but the error is plotted from t_c only.

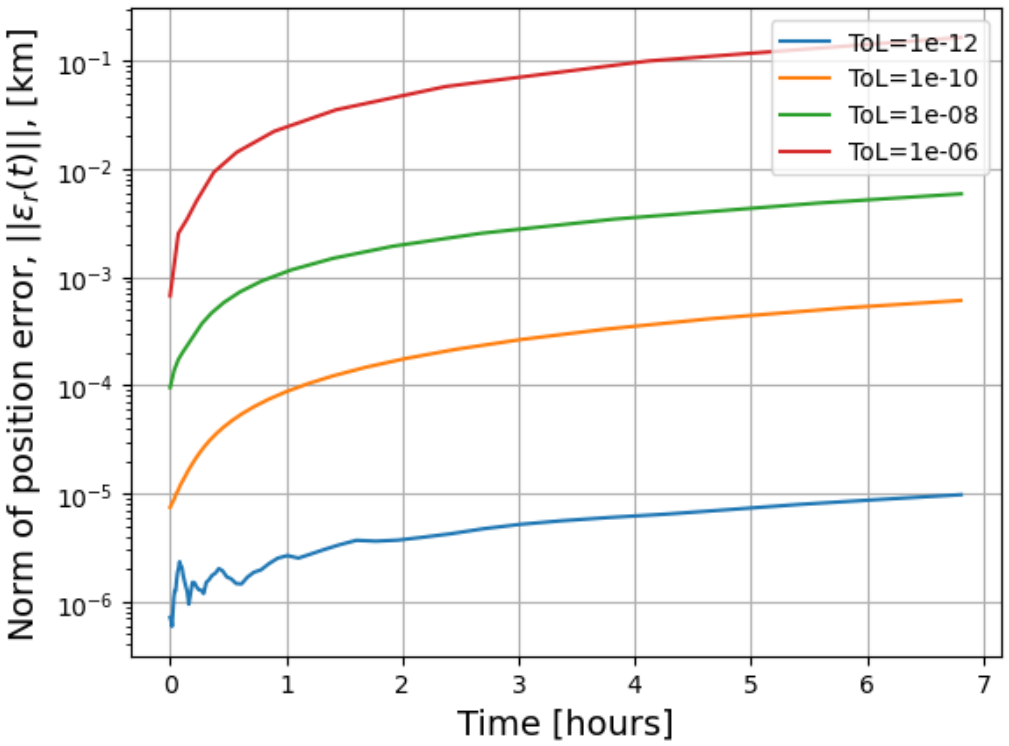

Figure 4.4: Perturbed Callisto flyby position error of the RKF5(6) variable time step integration using tolerances of 1e-12, 1e-10, 1e-8, and 1e-6, with respect to a benchmark computed with a fixed time step RKF7(8) method with $\Delta t = 1$s. The initial propagation time is set to t_0 (like in Q2), but the error is plotted from t_c only.

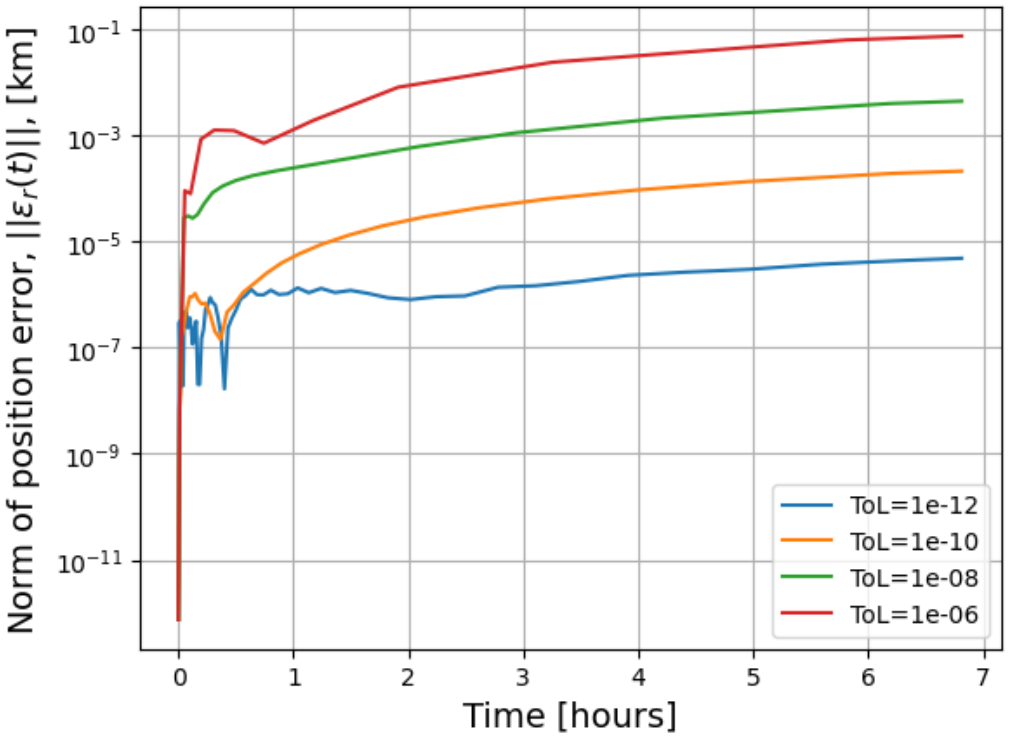

Figure 4.5: Perturbed Callisto flyby position error of the RKF5(6) variable time step integration using tolerances of 1e-12, 1e-10, 1e-8, and 1e-6, with respect to a benchmark computed with a fixed time step RKF7(8) method with $\Delta t = 1$s. The initial propagation time is set to t_c, but the error is plotted from t_c only.

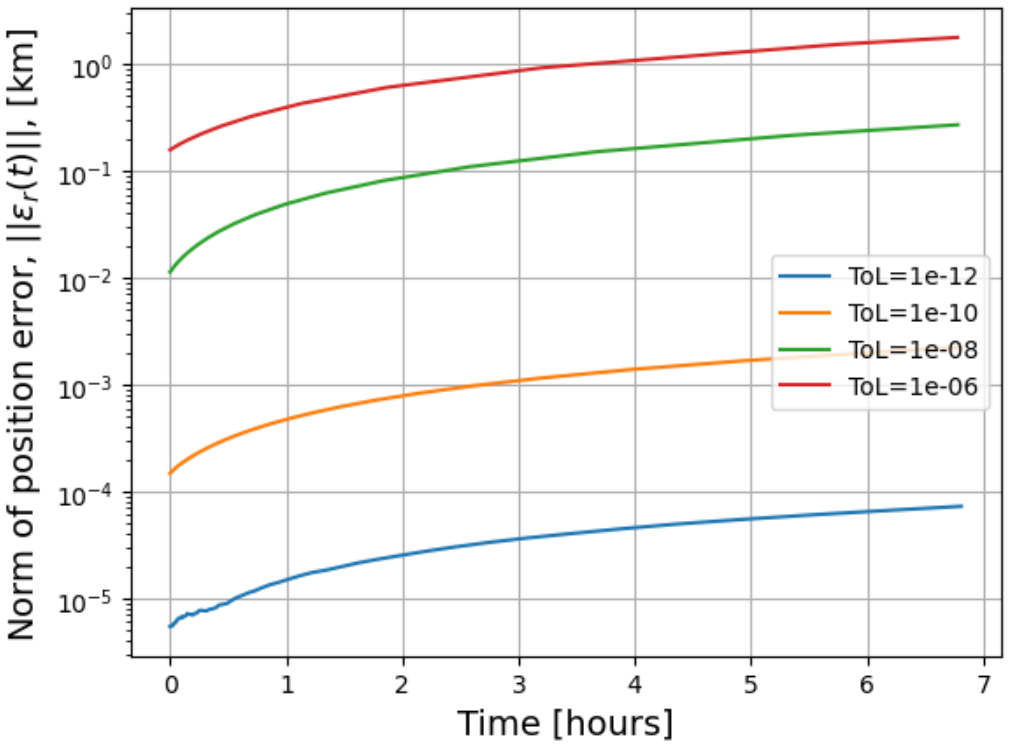

Figure 4.6: Perturbed Callisto flyby position error of the RKF5(6) variable time step integration using tolerances of 1e-12, 1e-10, 1e-8, and 1e-6, with respect to a benchmark computed with a fixed time step RKF7(8) method with $\Delta t = 1$s. The initial propagation time is set to $t_0 - 24$h, but the error is plotted from t_c only.

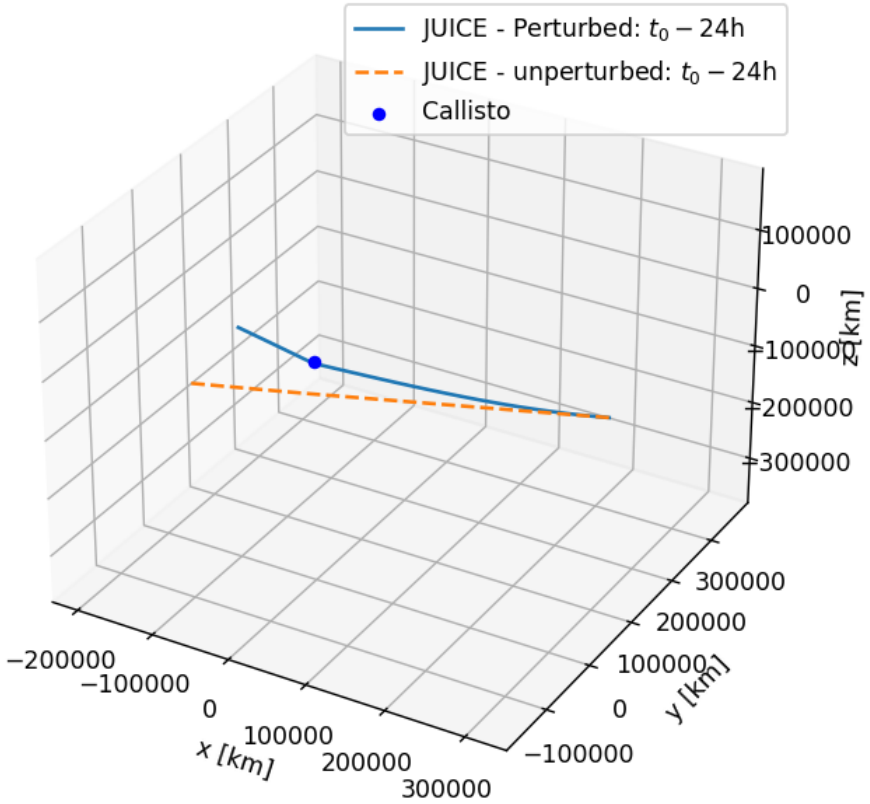

Figure 4.7: 3D plot of the trajectory of the $t_0 - 24$h propagations for both the perturbed and unperturbed Callisto flyby cases. This clearly shows that the unperturbed case is essentially a different trajectory.

Problem 5

5.1 LTE as a Function of Time - RKF7(8)

$$\begin{aligned} \boldsymbol{\epsilon}_{LTE}(t) &\approx \boldsymbol{K}(t)\Delta t^{p+1} \\ ||\boldsymbol{K_r}(t)|| &= \frac{||\boldsymbol{\epsilon}_{LTE,r}(t)||}{\Delta t^{p+1}} = \left|\left|\frac{\boldsymbol{\epsilon}_{LTE,r}(t)}{\Delta t^{p+1}}\right|\right| \end{aligned} \tag{5.1}$$

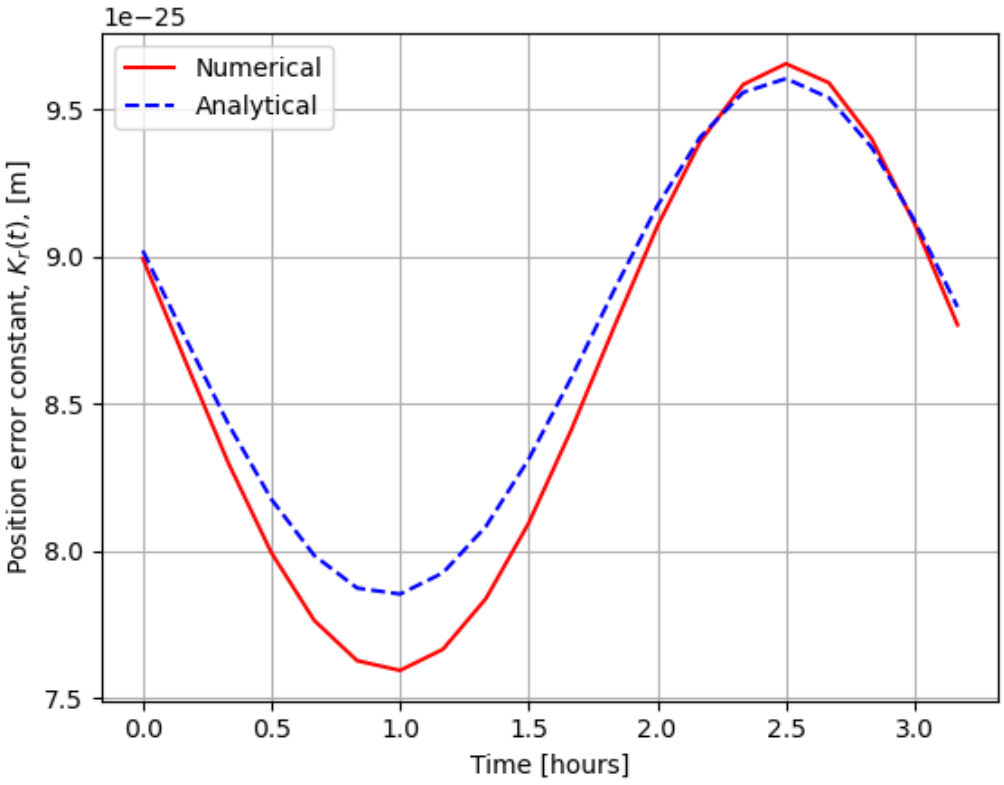

Figure 5.1: Local Truncation Error (LTE) as a function of time for the RKF7(8) method, computed based on 20 non-contiguous time steps of 300s.

5.2 Theoretical Value of $K_r(t)$

$$\begin{cases} x = R\cos(\omega t) \\ y = R\sin(\omega t) \end{cases} \tag{5.2}$$

$$\begin{cases} R = ||\boldsymbol{r_{G,s}}(t_0)|| \\ \omega = \sqrt{\frac{\mu_G}{||\boldsymbol{r_{G,s}}(t_0)||^3}} \end{cases} \tag{5.3}$$

$$\begin{cases} x = ||\boldsymbol{r_{G,s}}(t_0)||\cos\left(\sqrt{\frac{\mu_G}{||\boldsymbol{r_{G,s}}(t_0)||^3}}t\right) \\ y = ||\boldsymbol{r_{G,s}}(t_0)||\sin\left(\sqrt{\frac{\mu_G}{||\boldsymbol{r_{G,s}}(t_0)||^3}}t\right) \end{cases} \tag{5.4}$$

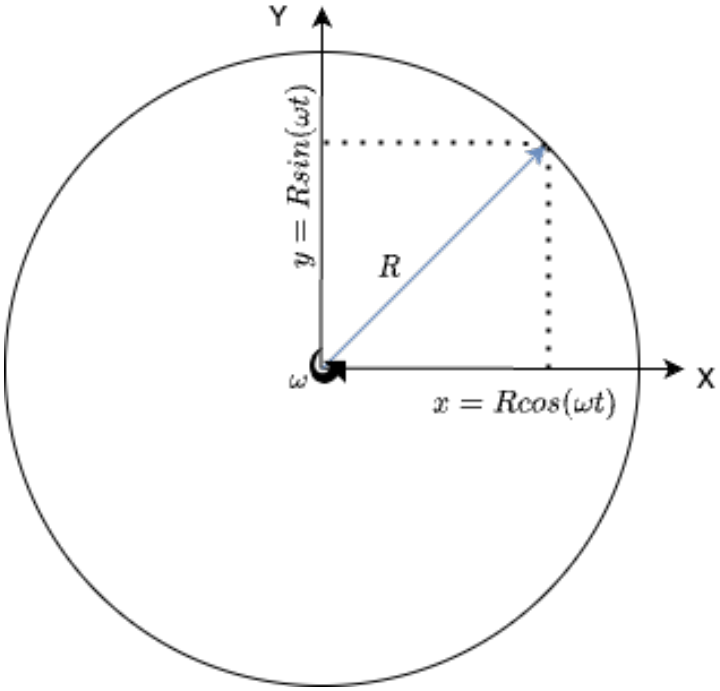

Figure 5.2: Uniform circular motion analytical solution. With $e = 0$, the orbit describes a 2D uniform circular motion with R the radius of the circle and ω the angular speed of the motion. The GCO500 orbit is then simplified at each epoch t_0 to a circular orbit with radius $||\boldsymbol{r}(t_0)||$ and angular speed equal to the mean motion.

$$\boldsymbol{\epsilon}_{LTE}(t) = \sum_{i=p+1}^{+\infty} \frac{\Delta t^i}{i!} \frac{d^i \mathbf{y}}{dt^i} \approx \frac{\Delta t^{p+1}}{(p+1)!} \frac{d^{p+1}\mathbf{y}}{dt^{p+1}} = \mathbf{K}(t)\Delta t^{p+1} \tag{5.5}$$

$$\frac{d^n}{dt^n}\left(\sin\left(\omega t\right)\right) = \omega^n \sin\left(\frac{n\pi}{2} + \omega t\right) \qquad \frac{d^n}{dt^n}\left(\cos\left(\omega t\right)\right) = \omega^n \cos\left(\frac{n\pi}{2} + \omega t\right)$$

$$\begin{cases} x = R\cos\left(\omega t\right) = R\sum_{i=0}^{+\infty} \frac{(t-t_0)^i}{i!}\omega^i \cos\left(\frac{i\pi}{2} + \omega t_0\right) = R\sum_{i=0}^{+\infty} \frac{\Delta t^i}{i!}\omega^i \cos\left(\frac{i\pi}{2} + \omega t_0\right) \\ y = R\sin\left(\omega t\right) = R\sum_{i=0}^{+\infty} \frac{(t-t_0)^i}{i!}\omega^i \sin\left(\frac{i\pi}{2} + \omega t_0\right) = R\sum_{i=0}^{+\infty} \frac{\Delta t^i}{i!}\omega^i \sin\left(\frac{i\pi}{2} + \omega t_0\right) \end{cases} \tag{5.6}$$

Comparing to $\boldsymbol{\epsilon}_{LTE}(t)$ yields Eq. (5.7), giving the analytical solution of the position components of the LTE.

$$\begin{cases} \epsilon_{LTE,x} = R\sum_{i=p+1}^{+\infty} \frac{\Delta t^i}{i!}\omega^i \cos\left(\frac{i\pi}{2} + \omega t_0\right) \\ \epsilon_{LTE,y} = R\sum_{i=p+1}^{+\infty} \frac{\Delta t^i}{i!}\omega^i \sin\left(\frac{i\pi}{2} + \omega t_0\right) \end{cases} \tag{5.7}$$

Using Eq. (5.5), Eq. (5.8) is obtained by taking the $i = (p+1)$ term of the Taylor expansion (dominant term). Additionally, Eq. (5.9) gives a more accurate formulation using terms until order n_{max} of the Taylor expansion.

$$\begin{aligned} ||\boldsymbol{K_r}(t)||_{dominant} = \frac{\sqrt{\epsilon_{LTE,x}^2 + \epsilon_{LTE,y}^2}}{\Delta t^{p+1}} &= \sqrt{\left(\frac{R\omega^{(p+1)}}{(p+1)!}\right)^2 \left(\sin\left(\frac{(p+1)\pi}{2} + \omega t_0\right)^2 + \cos\left(\frac{(p+1)\pi}{2} + \omega t_0\right)^2\right)} \\ &= \frac{R\omega^{(p+1)}}{(p+1)!} \\ &= \frac{||\boldsymbol{r_{G,s}}(t_0)||}{(p+1)!}\left(\sqrt{\frac{\mu_G}{||\boldsymbol{r_{G,s}}(t_0)||^3}}\right)^{p+1} \end{aligned} \tag{5.8}$$

$$||\boldsymbol{K_r}(t)||_{accurate} = \frac{\sqrt{\epsilon_{LTE,x}^2 + \epsilon_{LTE,y}^2}}{\Delta t^{p+1}} = \sqrt{R^2 \left(\left(\sum_{i=p+1}^{n_{max}} \frac{\Delta t^{i-(p+1)}}{i!} \omega^i \cos\left(\frac{i\pi}{2} + \omega t_0\right) \right)^2 + \left(\sum_{i=p+1}^{n_{max}} \frac{\Delta t^{i-(p+1)}}{i!} \omega^i \sin\left(\frac{i\pi}{2} + \omega t_0\right) \right)^2 \right)} \tag{5.9}$$

5.3 Numerical and Analytical Values of $K_r(t)$ for the Euler Integrator

$$||\boldsymbol{K_r}(t)||_{dominant} = \frac{||\boldsymbol{r_{G,s}}(t_0)||}{(2)!} \left(\sqrt{\frac{\mu_G}{||\boldsymbol{r_{G,s}}(t_0)||^3}} \right)^2 = \frac{1}{2!} \frac{\mu_G}{||\boldsymbol{r_{G,s}}(t_0)||^2} \tag{5.10}$$

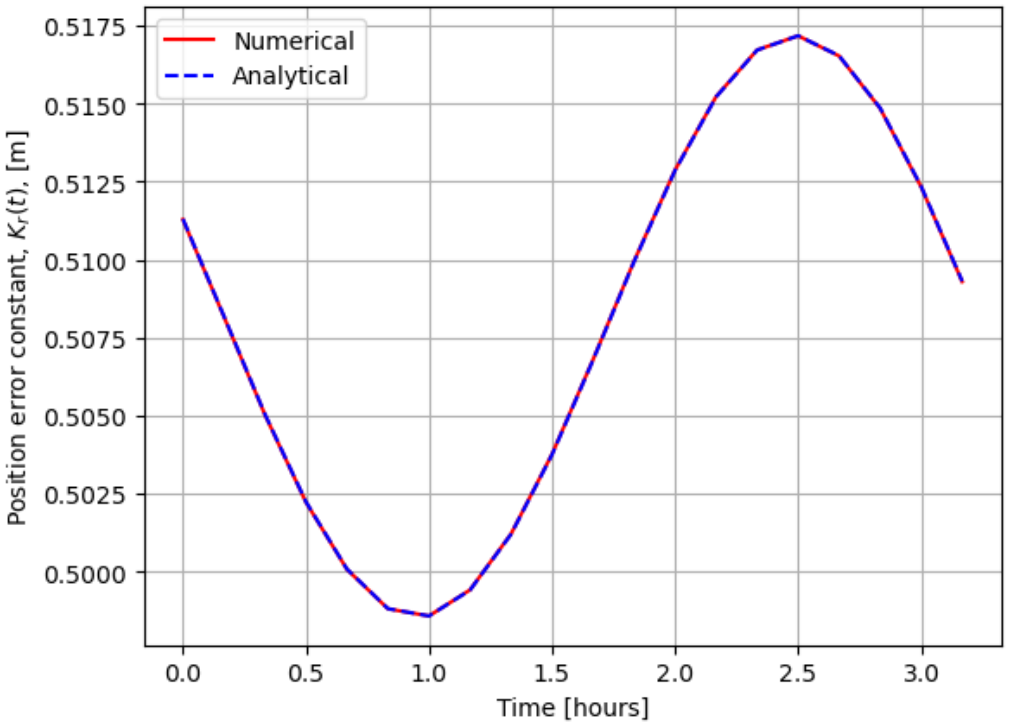

Figure 5.3: Local Truncation Error (LTE) as a function of time for the RKF7(8) method, computed based on 20 non-contiguous time steps of 10s. The analytical values of $\boldsymbol{K_r}(t)$ is given by Eq. (5.8) or (5.9), with p=1 for Forward Euler.

5.4 Discussion

For Euler, the analytical and numerical $||\boldsymbol{K_r}(t)||$ match nearly perfectly (offset of 1.75e-5 m on values of $\approx$ 0.5m). For RKF7(8), the match is less accurate, although it still captures the right magnitude, phase, and trends (sinusoidal motion). First, as the time step sizes considered are expected to be in the region where the LTE is dominant, mismatches mostly arise from the model used for the analytical solution. The true orbit deviates from a circle due to its eccentricity $e \approx 0.01$ (Tab. 5.1), meaning that $\boldsymbol{K_r}(t)$ will be different between the analytical and numerical solutions. Following, the reason the Euler scheme results in a better match can be shown through its dominant term of the position error constant (p=1, Eq. (5.11)), and the differential equation for an unperturbed orbit (Eq. (5.12), equation solved by TUDAT in Q5). Combining the two results in Eq. (5.13), which is clearly the same as Eq. (5.10) (evaluated at t_0). Note that the former was derived without any

assumption on the shape of the orbit (general 2D unperturbed orbit), while the latter is the analytical solution obtained from the circular orbit with angular speed equal to the mean motion. No similar link can be made for the RKF7(8) case, a higher accuracy of $\boldsymbol{K_r}(t)$ can only be obtained by improving the analytical model.

$$||\boldsymbol{K_r}_{Euler}(t)|| \approx \frac{1}{2!}\left|\left|\frac{d^2\boldsymbol{r_{G,s}}}{dt^2}\right|\right| \tag{5.11}$$

$$\frac{d^2\vec{r}}{dt^2} = \frac{-\mu_G}{||\vec{r}_{G,s}||^2}\hat{r}_{G,s} \tag{5.12}$$

$$||\boldsymbol{K_r}_{Euler}(t)|| \approx \frac{1}{2!}\frac{\mu_G}{||\boldsymbol{r_{G,s}}(t)||^2} \tag{5.13}$$

Table 5.1: Keplerian elements of the unperturbed GCO500 orbit.

a [km]	e [-]	i [°]	Ω [°]	ω [°]
3121.21	0.0092252	95.953	99.786	95.101

Problem 6

6.1 Error Extrapolation

Table 6.1: Variables used in the derivation of the error extrapolation method.

Variables	Meaning
$y(t)$	True, unknown, solution of the problem solved
$\bar{y}(t)$	Approximate solution obtained by a integrator (1 or 2 here)
$\epsilon(t)$	Error the approximate solution $\bar{y}(t)$ with respect to the real solution $y(t)$
Δt	Time step size
Subscript 1	RKF7(8) integrator with fixed time step Δt_1
Subscript 2	RKF7(8) integrator with fixed time step Δt_2
p	Order of the integrator used ($p = 7$ for RKF7(8))

$$y(t) = \bar{y}_1(t) + \epsilon_1(t;\Delta t_1) \qquad (6.1) \qquad\qquad y(t) = \bar{y}_2(t) + \epsilon_2(t;\Delta t_2) \qquad (6.2)$$

$$\begin{aligned} &\Leftrightarrow \bar{y}_1(t) + \epsilon_1(t;\Delta t_1) = \bar{y}_2(t) + \epsilon_2(t;\Delta t_2) \\ &\Leftrightarrow \bar{y}_1(t) - \bar{y}_2(t) = \epsilon_2(t;\Delta t_2) - \epsilon_1(t;\Delta t_1) \\ &\Leftrightarrow \bar{y}_1(t) - \bar{y}_2(t) = \epsilon_1(t;\Delta t_1)\left(\frac{\epsilon_2(t;\Delta t_2)}{\epsilon_1(t;\Delta t_1)} - 1\right) \end{aligned}$$

Assuming that the only difference between the two integrators is the time step size, and that both Δt's are small enough (first term of error definition is dominant) and chosen in the LTE dominant region (Fig. 1.3).

$$t > t_0 : \qquad \bar{y}_1(t) \neq \bar{y}_1(t) \qquad\qquad \epsilon_1(t) \neq \epsilon_2(t)$$

$$\begin{aligned} \frac{\epsilon_2(t;\Delta t_2)}{\epsilon_1(t;\Delta t_1)} &\approx \frac{N_2\epsilon_{LTE,2}}{N_1\epsilon_{LTE,2}} = \frac{N_2\epsilon_{LTE,2}}{\frac{\Delta t_2}{\Delta t_1}N_2\epsilon_{LTE,2}} \qquad N, \text{the number of time steps} \\ &= \frac{\Delta t_1}{\Delta t_2}\frac{\sum_{i=p}^{+\infty}\frac{\Delta t_2^i}{i!}\frac{d^i y(t)}{dt^i}}{\sum_{i=p}^{+\infty}\frac{\Delta t_1^i}{i!}\frac{d^i y(t)}{dt^i}} \\ &\approx \frac{\Delta t_1}{\Delta t_2}\frac{\frac{\Delta t_2^p}{(p)!}\frac{d^p y(t)}{dt^p}}{\frac{\Delta t_1^p}{(p)!}\frac{d^p y(t)}{dt^p}} \approx \left(\frac{\Delta t_2}{\Delta t_1}\right)^{p-1} \qquad p, \text{the LTE order} \end{aligned} \qquad (6.3)$$

$$\begin{aligned} &\Leftrightarrow \epsilon_1(t;\Delta t_1) = \frac{(\bar{y}_1(t) - \bar{y}_2(t))}{\left(\frac{\epsilon_2(t;\Delta t_2)}{\epsilon_1(t;\Delta t_1)} - 1\right)} \\ &\Leftrightarrow \epsilon_1(t;\Delta t_1) = \frac{(\bar{y}_1(t) - \bar{y}_2(t))}{\left(\left(\frac{\Delta t_2}{\Delta t_1}\right)^{p-1} - 1\right)} \end{aligned} \qquad (6.4)$$

It is clear from Fig. 6.1 that Eq. (6.4) gives a very accurate estimation of the position error for the $\Delta t_1 = 200$s propagation using the solution for $\Delta t_2 = 100$s. The percentage difference with the true error (from Keplerian orbit) can also be seen from Fig. 6.2, which shows that the extrapolation method is constantly within $\approx 0.04\%$.

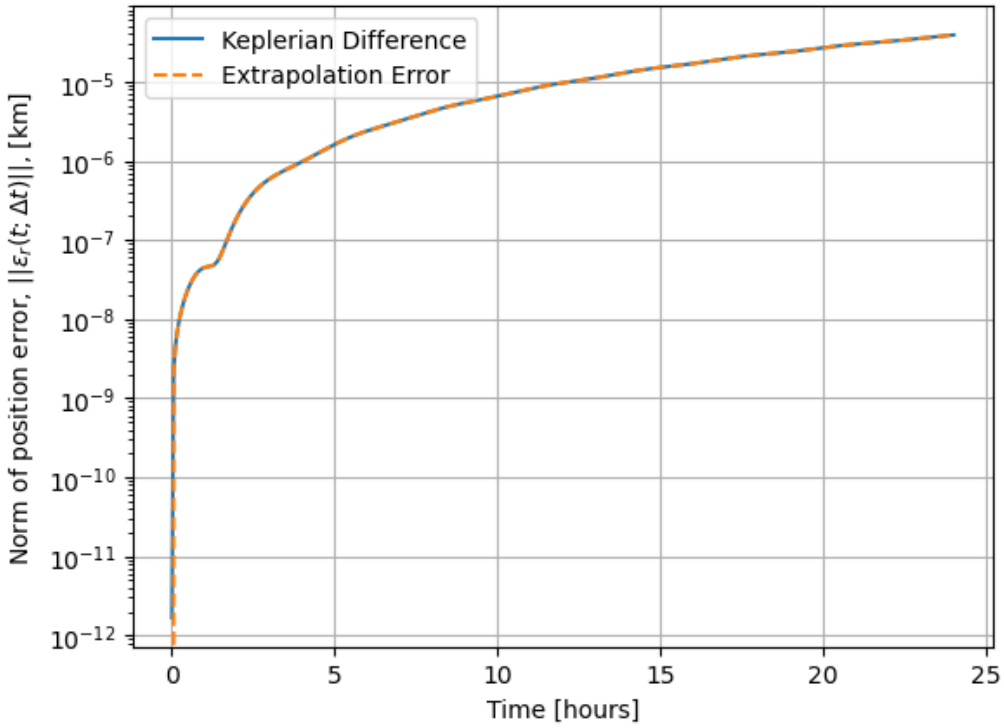

Figure 6.1: Position error in the unperturbed numerical propagation of the orbit around Ganymede for constant time steps of 200 seconds. The error is computed based on the extrapolation method with $\Delta t = 100$s as reference. Additionally, the error with respect to the analytical solution of the trajectory (Keplerian orbit) is plotted to assess the quality of the extrapolation method.

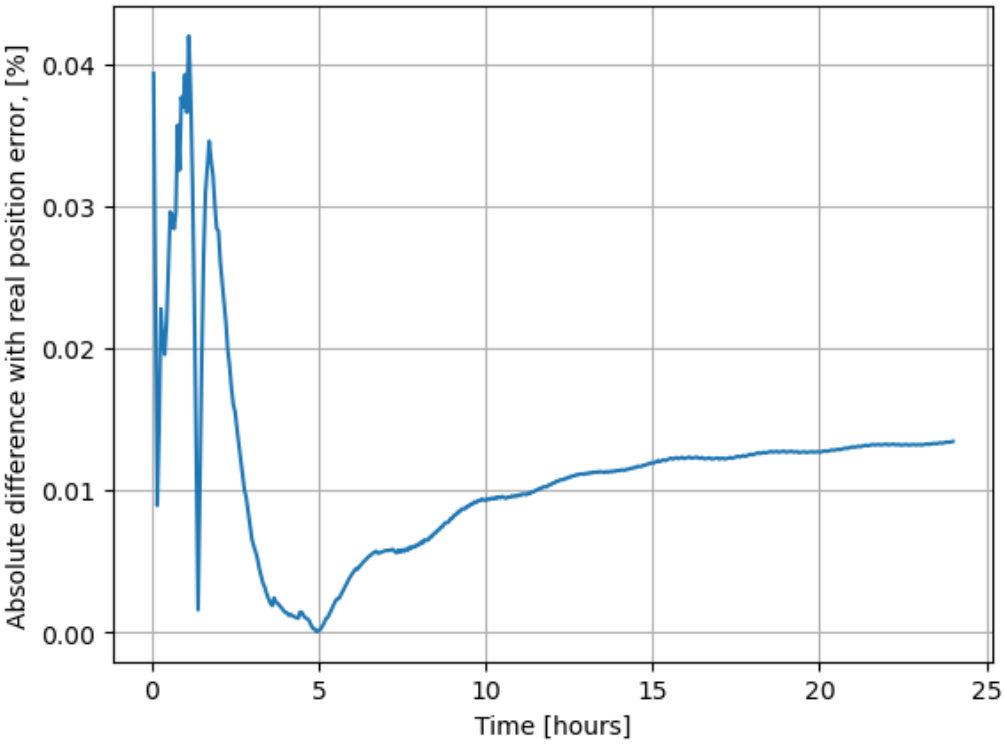

Figure 6.2: Percentage difference between the norms of position error predicted by the extrapolation method.

6.2 Application to Error of More Accurate Data

The derivation of the method only relied on two assumptions: both time step sizes are small enough and within the LTE dominance region. No assumption on the relative magnitude of the time steps was required, meaning that Eq. (6.4) can also be used to estimate the position error of $\Delta t = 100$s based on the $\Delta t = 200$s numerical solution (as both fall in the LTE region in Fig. 1.3). The difficulty in applying the method to estimate the error of the more accurate solution is in determining whether the Δt of the less accurate solution is small enough: taken too large, Eq. (6.3) may not be valid. In this respect, the estimation of the error for the lower accuracy propagation is more robust, as one only needs to ensure that $\bar{y}_2(t)$ is not in the rounding error region (easier to verify). The method is less accurate to estimate the $\Delta t = 100$s error, but still falls within 5% of the true value.

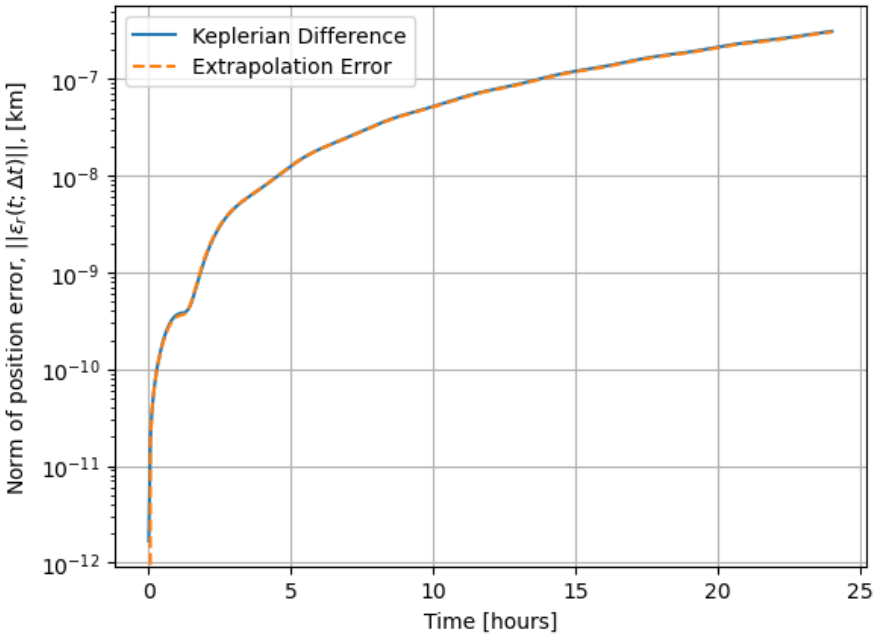

Figure 6.3: Position error in the unperturbed numerical propagation of the orbit around Ganymede for $\Delta t = 100$s (extrapolation method with respect to $\Delta t = 200$s).

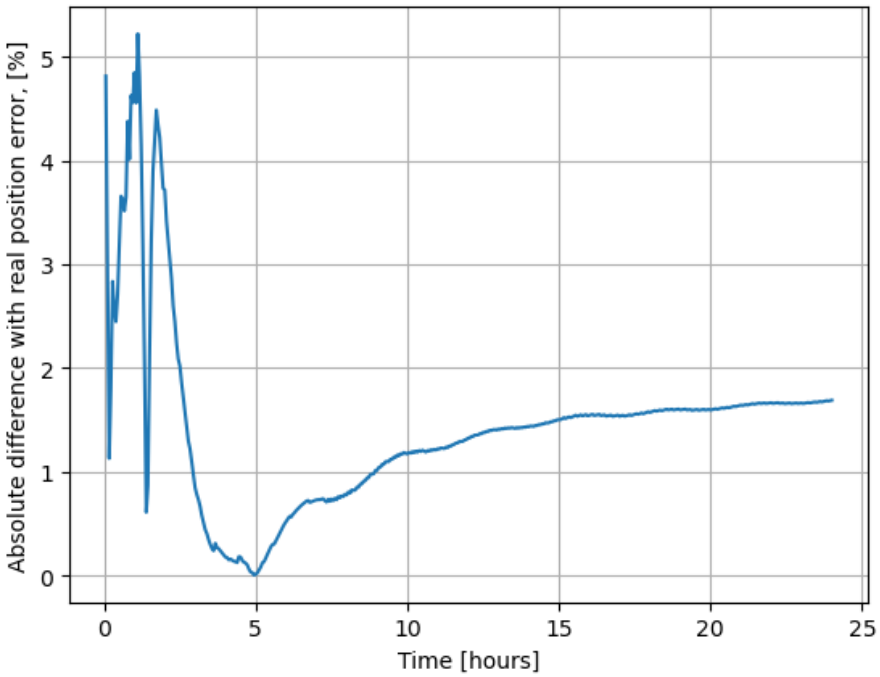

Figure 6.4: Percentage difference between the norms of position error predicted by the extrapolation method. The method is less accurate to estimate the $\Delta = 100$s error, but still falls within 5% of the true value.